2008

Study of Mechanical Loss Reduction on Thrust Bearings for Scroll Compressors Applying CO2 Refrigerant

Hideto Nakao
Mitsubishi Electric Engineering Corporation

Tetsuzo Matsugi
Mitsubishi Electric Engineering Corporation

Kenji Yano
Mitsubishi Electric Engineering Corporation

Katsunori Sato
Mitsubishi Electric Engineering Corporation

Study of Mechanical Loss Reduction on Thrust Bearings for Scroll Compressors Using CO_2 Refrigerant

Hideto NAKAO[1*], Tetsuzo MATSUGI[2], Kenji YANO[3], Katsunori SATO[4]

[1] Mitsubishi Electric Corporation, Advanced Technology R&D Center
Amagasaki-City, Hyogo, Japan
Phone: +81-6-6497-7582, Fax: +81-6-6497-7291, Postcode: 661-8661
E-mail: Nakao.Hideto@dr.MitsubishiElectric.co.jp

[2] Mitsubishi Electric Corporation, Air-Conditioning & Refrigeration System Works
Wakayama-City, Wakayama, Japan
Tel: +81-73-436-2121, Fax: +81-73-428-9022, Postcode: 640-8686
E-mail: Matsugi.Tetsuzo@da.MitsubishiElectric.co.jp

[3] Mitsubishi Electric Corporation, Air-Conditioning & Refrigeration System Works
Wakayama-City, Wakayama, Japan
Tel: +81-73-436-2121, Fax: +81-73-428-9022, Postcode: 640-8686
E-mail: Yano.Kenji@bc.MitsubishiElectric.co.jp

[4] Mitsubishi Electric Engineering Company Limited, Itami Engineering Office
Amagasaki-City, Hyogo, Japan
Tel: +81-6-6497-7278 Fax: +81-6-6428-3506, Postcode: 661-0001
E-mail: Sato.Katsunori@zc.MitsubishiElectric.co.jp

ABSTRACT

We have developed a scroll compressor employing CO_2 refrigerant, whose capacity is 9.4 kW. The CO_2 refrigerant has different characteristics from the refrigerants we have used for air-conditioning systems and refrigerators. There is particularly a large difference between the suction and discharge pressures of the CO_2 refrigerant. Therefore a large compression load is applied to the thrust bearing and the lubrication condition of the thrust bearing becomes critical. We have studied the lubrication of thrust bearings theoretically and experimentally. The average Reynolds equation by Patier & Cheng and the solid contact theories by Greenwood & Williamson and Greenwood & Tripp were used. The method of calculation and the adequacy of the calculated results were verified by model elemental experiments. The calculated frictional characteristics have properties similar to a Stribeck curve. The accurate configuration of the wedge film calculated improves the accuracy of the calculated frictional characteristics of the thrust bearing.

1. INTRODUCTION

There is a large difference between the suction and discharge pressure of CO_2 refrigerant. Therefore a large compression load is applied to the thrust bearing. The oil film thickness has to be maintained thick enough to prevent the film on the thrust bearing disappearing and the mechanical loss on the thrust bearing has to be reduced in order to facilitate highly-efficient scroll compressors. Some studies on thrust bearings in scroll compressor are reported.

Nishiwaki et al. (1996) presented an experimental study for the lubrication of thrust bearings in a refrigerant atmosphere. The friction loss of thrust bearing rises, when the rotational frequency and the load are increased. However the friction coefficient is kept at a constant value.

Oku et al. (2006) presented the film formations and the friction loss of thrust bearings by experiments in a high pressure atmosphere and mathematical simulations. However their thrust bearing investigations were on special formation loading back pressure.

It has to bring out the relationship between the dimensions and the operating conditions of the thrust bearing and the frictional characteristics in order to design a low friction loss thrust bearing. Therefore we have simulated the friction coefficient of a thrust bearing using the average Reynolds equation by Patier & Cheng (1978, 1979) and the solid contact theories by Greenwood & Williams and Greenwood & Tripp (1966, 1970-71). We have also evaluated the adequacies of simulating the results by model experiments.

2. EXPERIMENTS OF THRUST BEARING

2.1 Experimental Apparatus

Figure 1 shows the experimental apparatus. The oil-filled lower holder is set on two orthogonal linear guides. The ring-like lower test specimen is fixed on the lower holder. The lower holder is orbiting, revolved by the rotating crank shaft. The circular upper test specimen is fixed on the under surface of the upper holder restraining rotation. The upper holder is supported by a steel boll in order to keep the parallelism of the test specimens. The test specimens are submerged in the oil. The test load acts on the center of crank shaft. The horizontal eccentric offset distance between the centers of the lower specimen and crank shaft is 2 mm. The vertical test load and the horizontal friction load changing direction with each crank angle act on the test specimens. These loads are measured by a three dimensional load cell set against the upper holder.

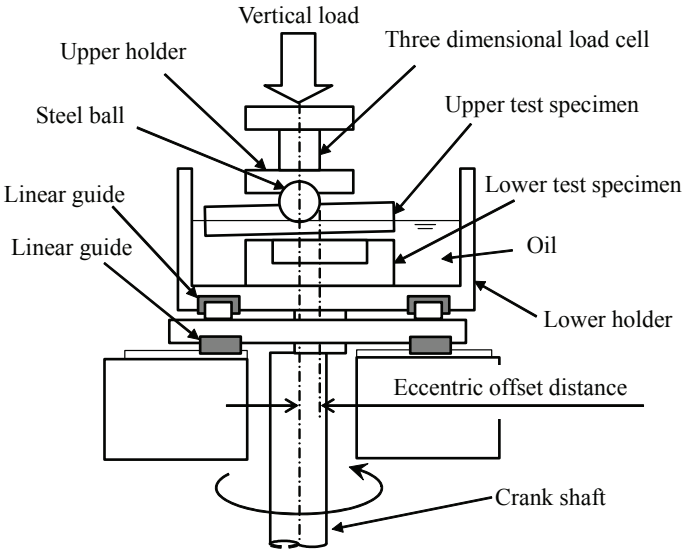

Figure 1 Experimental apparatus

2.2 Test Specimens

Table 1 shows the dimensions of upper and lower test specimens.

Table 1 Dimensions of upper and lower test specimens

	Upper	Lower
Material	Cast iron	Cast iron
Outer diameter	ϕ50 mm	ϕ40 mm
Internal diameter	——	ϕ16 mm, ϕ32 mm
Thickness	5 mm, 13 mm	——

2.3 Experimental Conditions

Table 2 shows the experimental conditions. The revolutions of the crank shaft are kept at the set value for five seconds and the vertical load and horizontal friction load are measured in these five seconds. The data sampling rate was 10 s^{-1} in experiments. The experiments were conducted in the oil.

Table 2 Experimental conditions

Revolutions	1, 3, 10, 20, 30, 40, 50 s^{-1}
Vertical load	250, 500, 750, 1000 N
Viscosity coefficient	8 mPa・s

3. THEORETICAL ANALYSIS OF THRUST BEARING

3.1 Theoretical Analysis Model

Figure 2 shows the theoretical analysis model that simulated the experimental apparatus. The vertical load makes the upper test specimen sag downwards in the center and the lower test specimen orbiting revolves around O_J which is the center of the crank shaft. The lower test specimen does not change its attitude and the X_S-Y_S coordinate whose origin is O_S rotates around O_J which is the origin of X_J-Y_J coordinate. The sliding direction changes with each crank angle and the sliding velocity is a constant value.

The vertical load acts on O_J which is the centers of the crank shaft and the upper test specimen. The upper test specimen is supported at the center of itself. The maximum film thickness is formed at the point inclined at θ_c angle from the X_S axis, because the vertical load is acting on the eccentric point from O_J and the sliding direction is

changing with each crank angle change. The oil film pressure is generated between the upper and lower test specimens, because the upper test specimen is deformed by the vertical load and the upper and lower test specimens move apparently with each other. Partial contact pressure is generated, when the film thickness approaches approximately the surface roughness.

Figure 3 shows the loads and the moments acting between the upper and lower test specimens. The oil film pressure and the partial contact pressure act so these resultant forces balance with the vertical load.

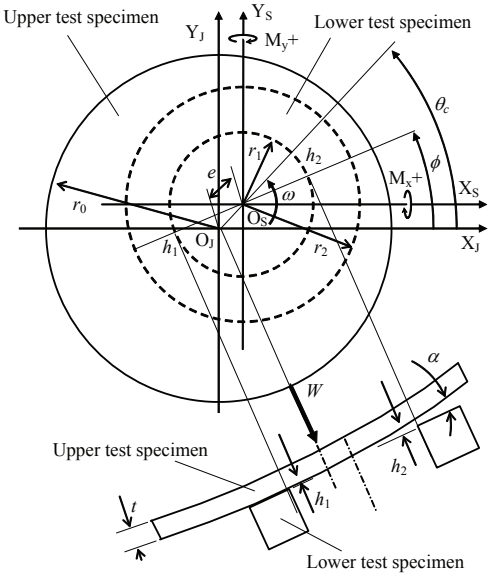

Figure 2 Theoretical analysis model that simulated the experimental apparatus

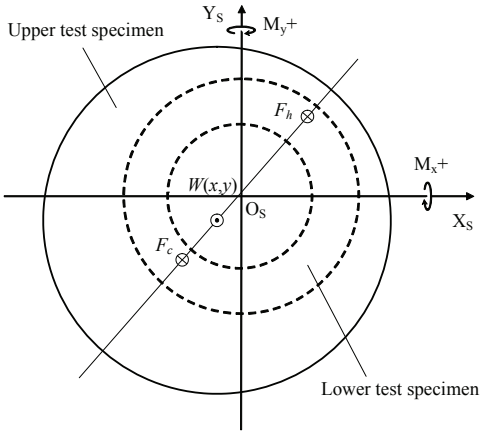

Figure 3 Loads and moments acting between upper and lower test specimens

3.2 Film Thickness

The minimum film thickness at the inside of the lower test specimen is h_1. The maximum film thickness is h_2. The angle of inclination of the upper test specimen at the inside of the lower test specimen is α presented in figure 2. The oil film thickness h between the upper and lower test specimens are calculated by function (1).

$$h = \frac{h_2 - h_1}{2r_1}\{r\cos(\theta - \phi) + r_1\} + h_1 + (r - r_1)\sin\alpha \qquad r_1 \le r \le r_2 \tag{1}$$

Here, α is calculated by functions (2).

$$\alpha = \frac{W \cdot r_1}{8\pi D}, \qquad D = \frac{E \cdot t^3}{12(1-\nu^2)} \tag{2}$$

3.3 Average Reynolds Equation

The viscosity coefficient, the density of lubrication oil and the oil flow velocities for the X and Y axial directions are a constant value. The average Reynolds equation with random roughness given by Patier & Cheng (1978, 1979) is as function (3).

$$\frac{1}{\eta}\left\{\frac{\partial}{\partial x}\left(\phi_x h^3 \frac{\partial p}{\partial x}\right) + \frac{\partial}{\partial y}\left(\phi_y h^3 \frac{\partial p}{\partial y}\right)\right\} = 12\frac{\partial \phi_c h}{\partial t} + 6\left\{U\left(\frac{\partial \phi_c h}{\partial x} + \sigma\frac{\partial \phi_s}{\partial x}\right) + V\left(\frac{\partial \phi_c h}{\partial y} + \sigma\frac{\partial \phi_s}{\partial y}\right)\right\} \tag{3}$$

3.4 Oil Reaction Force and Moment

The oil reaction force F_h and the moments of the oil reaction force M_{hx} and M_{hy} are calculated by function (3). They are shown from functions (4) to (6).

$$F_h = \int_{r_1}^{r_2}\int_{0}^{2\pi} pr\,d\theta\,dr \quad (4) \qquad M_{hx} = \int_{r_1}^{r_2}\int_{0}^{2\pi} pr^2 \sin\theta\,d\theta\,dr \quad (5)$$

$$M_{hy} = \int_{r_1}^{r_2}\int_{0}^{2\pi} pr^2 \cos\theta\,d\theta\,dr \quad (6)$$

3.5 Solid Contact Force and Moment

Partial contact occurs, when the film thickness approaches approximately the surface roughness. Using the contact models given by Greenwood & Williams (1966) and Greenwood & Tripp (1970), the solid contact force F_c is calculated by function (7).

$$F_c = \pi(\lambda\beta\sigma_a)A_0 H_d F(h/\sigma_a) \quad (7)$$

Here, $F(a)$ is the probability density function and it is given by function (8).

$$F(a) = \frac{1}{\sqrt{2\pi}}\int_{a}^{\infty}(u-a)\exp(-u^2/2)du \quad (8)$$

The solid contact pressure p_c is given by function (9), using function (7).

$$p_c = \pi(\lambda\beta\sigma_a)H_d \cdot F(d/\sigma_a) \quad (9)$$

The actual contact area A_r is given by function (10).

$$A_r = \pi(\lambda\beta\sigma_a)A_0 \cdot F(d/\sigma_a) \quad (10)$$

In the case of plastically contact, A_r is calculated by function (11), using the plastic flow pressure p_m.

$$A_r = \frac{F_c}{p_m} \quad (11)$$

The density of surface asperities λ and the top radius of surface asperity β need to be measured in order to calculate the solid contact force and the actual contact area. These were measured as a three dimensional surface roughness using a laser microscope.

The solid contact force F_c is calculated by function (12).

$$F_c = \pi(\lambda\beta\sigma_a)\int_{r_1}^{r_2}\int_{0}^{2\pi} F_1(h/\sigma_a)r\,d\theta\,dr \quad (12)$$

The moments generated by the solid contact force M_{cx}, M_{cy} are calculated by functions (13) and (14).

$$M_{cx} = \pi(\lambda\beta\sigma_a)\int_{r_1}^{r_2}\int_{0}^{2\pi} F_1(h/\sigma_a)r\sin\theta\,d\theta\,dr \quad (13)$$

$$M_{cy} = \pi(\lambda\beta\sigma_a)\int_{r_1}^{r_2}\int_{0}^{2\pi} F_1(h/\sigma_a)r\cos\theta\,d\theta\,dr \quad (14)$$

3.6 Friction Coefficient

The friction coefficient of the upper test specimen μ is given by function (15). Here, the fluid friction force acting on the smallest area of the upper test specimen is F_{fh} and the contact friction force of upper test specimen is F_{fc}. These are given by functions from (16) to (20).

$$\mu = \frac{F_{fh} + F_{fc}}{W} \tag{15}$$

$$F_{fc} = A_r \cdot s \tag{16}$$

$$F_{fh} = \int_{r_1}^{r_2} \int_{0}^{2\pi} f_{fh} \cdot r d\theta dr \tag{17}$$

$$f_{fh} = \sqrt{f_x^2 + f_y^2} \tag{18}$$

$$f_x = -(\phi_f - \phi_s)\frac{\eta U}{h} - \phi_{fp}\frac{h}{2}\left(\cos\theta\frac{\partial p}{\partial r} - \frac{\sin\theta}{r}\frac{\partial p}{\partial \theta}\right) \tag{19}$$

$$f_y = -(\phi_f - \phi_s)\frac{\eta U}{h} - \phi_{fp}\frac{h}{2}\left(\sin\theta\frac{\partial p}{\partial r} + \frac{\cos\theta}{r}\frac{\partial p}{\partial \theta}\right) \tag{20}$$

3.7 Calculation Conditions

Table 3 shows the calculation conditions and table 4 shows the actual measurement values of surface roughness. The surface roughness is defined as non-dimensional random form.

Table 3 Calculation conditions

Thickness of upper test specimen	13 mm
Internal diameter of lower test specimen	ϕ16 mm, ϕ 32 mm
Outer diameter of lower test specimen	40 mm
Eccentric offset distance of main shaft	2 mm
Young's modulus	170.6 GPa
Poisson ratio	0.3
Viscosity coefficient	8 mPa·s

Table 4 Actual measurement values of surface roughness

Test specimen	Upper	Lower
Density of surface asperity	1319 /mm^2	3207 /mm^2
Top radius of surface asperity	51.7 μm	45.7 μm
Root-mean-square deviation of height	0.115 μm	0.182 μm
Plastic flow pressure	2.70 GPa	2.18 GPa
Root-mean-square height	0.448 μm	0.487 μm
Average of height	0.050 μm	0.161 μm

4. CHARACTERITICS OF THRUST BEARINGS

4.1 Experimental Results

Figure 4 shows the friction coefficients of the thrust bearing in the experiment. The friction coefficients are the highest at the 1 s^{-1} of rotational frequency and the friction coefficients descend, when the bearing characteristics number rises a little. The friction coefficients rise again in the high range of bearing characteristic numbers. These frictional characteristics have properties similar to a Stribeck curve. The wedge film is formed by the deformation of upper test specimen in the case of bearing pressure is a higher value.

The wedge film is not formed because the sliding surfaces are keeping parallel in the case of low bearing pressure and the deformation volume is small. However the frictional characteristics have properties similar to a Stribeck curve. Lebeck presents that plane bearings have characteristics of a Stribeck curve similar to the inclined plane bearings from experimental data of many researches (1987). There is no theory which explains this mechanism. Our experimental results have the mechanism similar to plane bearings of Lebeck.

The friction coefficient in the case of thickness of the upper test specimen of 5 mm is greater than 13 mm specimen at the same vertical load. It is for this reason that the shear load rises in the adhesive area because the deformation of upper test specimen degrades the degree of parallelization in the upper and lower test specimens and the actual contact area expands. Therefore the friction coefficient reduces in the case when the deformation volume

of thrust bearing is smaller. The friction coefficient reduces in the case when the internal diameter of lower test specimen is smaller. It is for this reason that the effective area expands, when the internal diameter of the lower test specimen is smaller.

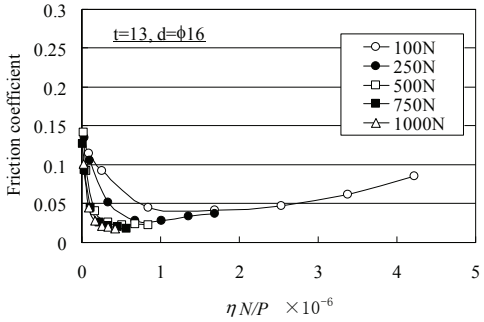

Internal diameter ϕ16 mm, Thickness 13 mm

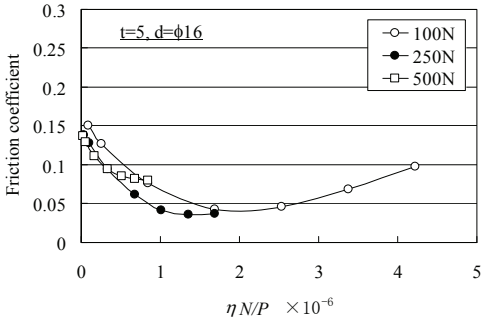

Internal diameter ϕ16 mm, Thickness 5 mm

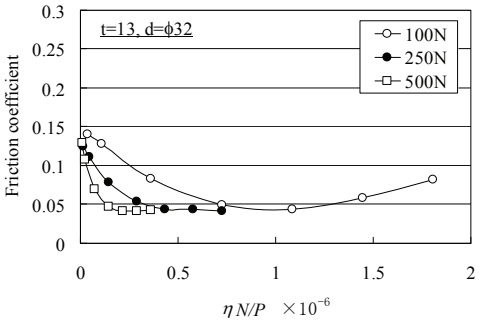

Internal diameter ϕ32 mm, Thickness 13 mm

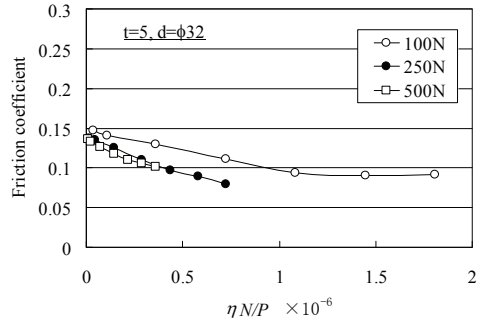

Internal diameter ϕ32 mm, Thickness 5 mm

Figure 4 Friction coefficients of the thrust bearing in the experiments

4.2 Calculation Results

Figure 5 shows the relationship between the experimental and calculated friction coefficients. Here, the thickness of upper test specimen is 13 mm.

In the case where the internal diameter of the lower test specimen is 16 mm and the bearing characteristic number is the same value, the calculated friction coefficient reduces, when the vertical load is larger. The calculated friction coefficient also approaches the constant value, when the bearing characteristic number rises. The experimental results denote the same tendency of the calculated results and the method of calculation is therefore appropriate.

In the case where the internal diameter of the upper test specimen is 32mm and the bearing characteristic number is the same value, the calculated friction coefficient reduces, when the vertical load is larger. The calculated friction coefficient is a constant value, when the bearing characteristic number rises. However the experimental friction coefficient decreases, when the bearing characteristic number rises.

Figure 6 shows the relationships between the bearing characteristic number and the oil reaction force, the solid contact force in the case of the diameters of the upper test specimens were 16 mm and 32 mm. Figure 7 also shows the relationships between the bearing characteristic number, the fluid friction force and the contact friction force in the case of the same conditions. The vertical load was 250 N in the calculated conditions of figure 6 and 7. The calculated friction coefficient is based on the friction force resulting from the fluid friction force and the contact friction force. The solid contact force reduces, in the case when the bearing characteristic number rises and the oil reaction force increases, so the film thickness becomes thicker. Therefore the calculated fluid friction force increases and the contact friction force decreases in the case of internal diameter is 16 mm and the bearing characteristic number is the high value. However the calculated contact friction force is the high and constant value in the case of internal diameter is 32 mm and the bearing characteristic number is a high value. The contact friction force is a constant value in the case of the bearing characteristic number changes, because the contact friction force does not come under the influence of the sliding velocity.

The difference between the calculated and experimental results becomes greater, when the solid contact force increases because the contact theory is more inaccurate than the fluid lubrication theory. Therefore the calculated results correspond with the experimental results in the conditions of the diameter of the upper test specimen at 16 mm, mainly because of fluid lubrication.

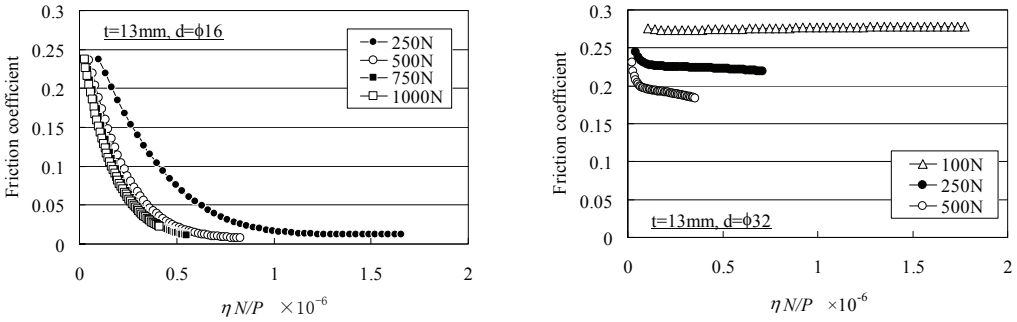

Internal diameter ϕ16 mm, Thickness 13 mm Internal diameter ϕ32 mm, Thickness 13 mm

Figure 5 Relationship between experimental and calculation friction coefficients

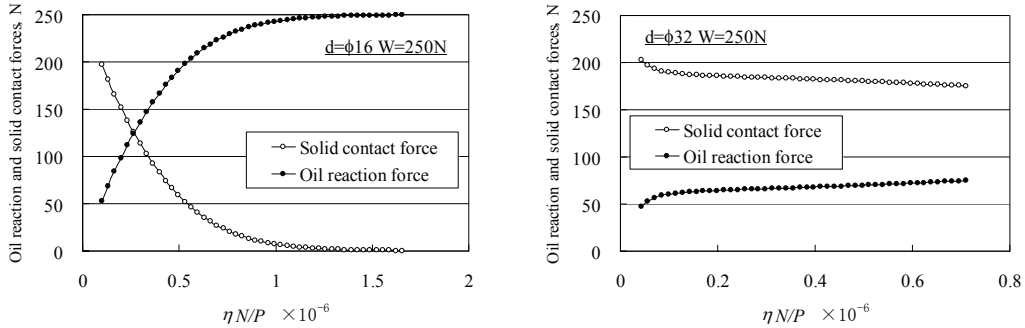

Figure 6 Relationships between bearing characteristic number, oil reaction force and solid contact force (t =13 mm, W=250 N)

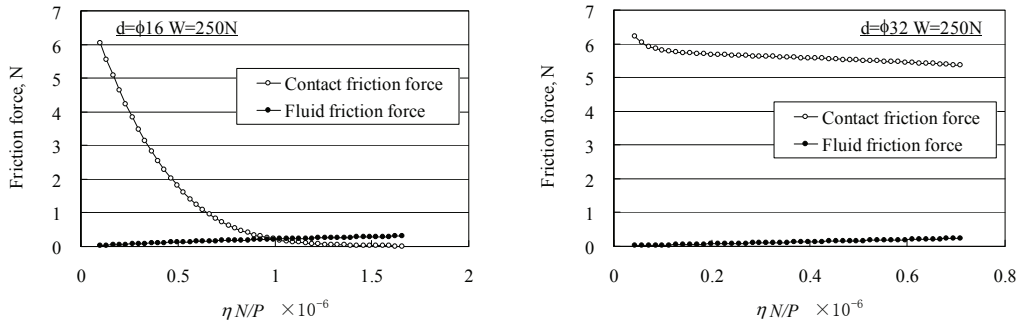

Figure 7 Relationships between bearing characteristic number, fluid friction force and contact friction force (t =13 mm, W=250 N)

5. CONCLUSIONS

In order to understand the supporting load mechanism of thrust bearings in a scroll compressor, we have built a thrust bearing model which was constructed by the oil reaction force based on the fluid mechanics and solid contact force including the roughness of the sliding surfaces. We also compared the calculated results with the experimental results. The following conclusions were obtained from the results of the studies.

- The frictional characteristics of the orbiting movement have properties similar to a Stribeck curve.
- The friction coefficient depends on the theory combined in the oil reaction force by the mixed lubrication and the solid contact force including the roughness of sliding surfaces, this corresponded with the experimental results that simulated the thrust bearing in the scroll compressor qualitatively.
- The simulated results correspond to the experimental results within the range when the solid contact force is small.
- The most optimum elastic deformation volume of thrust bearing and the most optimum configuration makes this thrust bearing highly-efficient.

NOMENCLATURE

A_r	actual contact area	A_0	apparent contact area
E	Young's modulus	F_c	solid contact force
F_{fc}	solid friction force	F_{fh}	fluid friction force
F_h	fluid reaction force	H_d	Vickers hardness
h	nominal oil film thickness		
h_1	minimum film thickness at the inside of lower test specimen		
h_2	maximum film thickness	h_{min}	minimum film thickness
N	rotational frequency of crank shaft	P_c	solid contact pressure
p_m	plastic flow pressure	s	shear strength
r_1	internal diameter of lower test specimen	r_2	outer diameter of lower test specimen
U , U_c , V	boundary velocity	W	vertical load
X , Y	coordinates	α	inclination angle
β	top radius of surface asperity	ϕ	inclination angle
ϕ_c , ϕ_x , ϕ_y , ϕ_s , ϕ_{fp}	flow factor	η	oil viscosity
λ	density of surface asperities	μ	friction coefficient
ν	Poisson ratio	θ	orbiting angle
θ_c	crank angle	σ	root-mean-square height
σ_a	root-mean-square deviation of height		

REFERENCES

Nishiwaki, F., Hasegawa, H., Ikoma, M., Matsuzaki, R. & Muramatsu, S., 1996, Mechanical Loss Reduction at Thrust Bearings of Scroll Compressors Using R407C, *International Compressor Engineering Conference at Purdue*, p.263-268.

Oku, T., Anami, K., Ishii, N., Ishii, N., Knisely, C. W., 2006, Optimal performance design method of thrust slide-bearing in scroll compressors for its best efficiency, *International Compressor Engineering Conference at Purdue*, C128.

Patier, N., Cheng, H. S., 1978, An average flow model for determining effects of three dimensional roughness onpartial hydrodynamic lubrication, *Transactions of the ASME* , Vol. 100, p12-17.

Patier, N., Cheng, H. S., 1979, Application of average flow model to lubrication between rough sliding surfaces, *Transactions of the ASME* , Vol. 101, p. 220-230.

Greenwood, J.A., Williamson, J.B.P., 1966, Contact of nominally flat surfaces, *Proc. R. Soc., London, Ser. A, Vol. 295*, p. 300-319.

Greenwood, J. A., Tripp, J. H., 1970-71, The Contact of two nominal flat rough surfaces, *Proc. Inst. Mech. Engrs.*, vol. 185, 48/71, p. 625-633.

Lebeck, A. O., 1987, Parallel sliding load support the mixed friction regime part 1 the experimental data, *ASME Journal of tribology*, vol.109, p. 189-195.